

Minimal Integer Automaton behind Crystal Plasticity

Oğuz Umut Salman¹ and Lev Truskinovsky^{1,2}

¹LMS, CNRS-UMR 7649, Ecole Polytechnique, Route de Saclay, 91128 Palaiseau, France

²SEAS, Harvard University, 29 Oxford Street, Cambridge, Massachusetts 02138, USA

(Received 23 February 2011; published 29 April 2011)

Power law fluctuations and scale-free spatial patterns are known to characterize steady state plastic flow in crystalline materials. In this Letter we study the emergence of correlations in a simple Frenkel-Kontorova-type model of 2D plasticity which is largely free of arbitrariness, amenable to analytical study, and is capable of generating critical exponents matching experiments. Our main observation concerns the possibility to reduce continuum plasticity to an integer-valued automaton revealing inherent discreteness of the plastic flow.

DOI: 10.1103/PhysRevLett.106.175503

PACS numbers: 62.20.fq, 46.35.+z, 81.16.Rf, 81.40.Lm

At the macroscale one usually assumes that crystalline materials flow plastically when averaged stresses exceed yield thresholds. At the microscale plasticity evolves through a sequence of slow-fast events involving collective pinning and depinning of dislocational structures. Classical engineering theory has been very successful in reproducing the most important plasticity phenomenology such as yield, hardening, and shakedown; however, a fully quantitative link between the phenomenological theory and the microscopic picture of plasticity remains elusive. The main reason is that the phenomenological approach implies spatial and temporal averaging in the system with poorly understood long-range correlations.

The presence of such correlations has been confirmed by numerous experiments revealing intermittent character of plastic activity with power law statistics of avalanches and self-similar structure of dislocation cell structures [1]. The emergence of power laws suggests that in plasticity the relation between the microscopic and the macroscopic models is more akin to turbulence than to elasticity [2]. Similar critical features of stationary nonequilibrium states have been observed in a variety of other driven systems with threshold nonlinearity and rate independent dissipation; however, the problem of classifying the universality classes remains largely open [3]. In this situation, finding the minimal representation of each class that is amenable to rigorous analysis is of significant general interest.

The experimental evidence of plastic criticality has been corroborated by several numerical models [4]. The two main microscopic approaches are discrete dislocation dynamics (DDD), accounting for dislocation interactions on different slip planes [5–7], and a pinning-depinning model dealing with plasticity on a single slip plane [8,9]. Different mesoscopic continuum models implying partial averaging have also been shown to generate power law statistics of avalanches with realistic exponents [2,10]. Since scale-free dislocation activity is expected to be independent of either microscopic or macroscopic details, one can try to maximally simplify the underlying physics

while still capturing the observed exponents and even characteristic shape functions [11]. Presently the only analytically tractable models of plasticity are the mean field theory [12,13], the renormalization group models of elastic depinning [14], and the Abelian automata of sandpile type [15]. In this group only the automata models have a potential of capturing the whole complexity of the dislocation patterning, and the goal of this Letter is to propose a formal reduction of a realistic plasticity model to a spin model with discrete time evolution. Instead of straightforward time discretization of continuum dynamics [16], we search for *inherent* temporal discreteness hidden behind the conventional gradient flow dynamics [17].

While the 1D automata, describing successfully plastic hysteresis and rate independent dissipation, fall short of capturing plastic criticality [17], the 2D automaton-based models may already be adequate at least for fcc and hexagonal crystals; it is also noteworthy that intermittency has been mostly observed under single slip conditions [12,18]. In such cases one can get a realistic model by assuming that plasticity proceeds through the motion of a set of parallel edge dislocations. We further neglect the vectorial nature of the problem and reduce the crystal to an array of coupled Frenkel-Kontorova (FK) chains [19]. In contrast to more conventional DDD modeling [5], where nucleation and propagation rules are not associated with the same thresholds, the FK-type models describe adequately both the multiplication of the defects and their kinetics including the finite size of the Peierls stress [20].

To describe the model we first recall that classical continuum dislocation mechanics deals with the energy $\Phi(u) = \int \bar{\phi}(\nabla u)$, where $u(x)$ is the displacement field and the function $\bar{\phi}$ is quadratic. The displacement field is allowed to have finite discontinuities $[u]$ whose evolution is governed by phenomenological kinetic relations [21]. The atomic structure of dislocations can be addressed by introducing an internal length scale a (Burgers parameter) and replacing continuum energy by the discrete one, which can be schematically represented as $\Phi(u) = a \sum \phi([u]/a)$

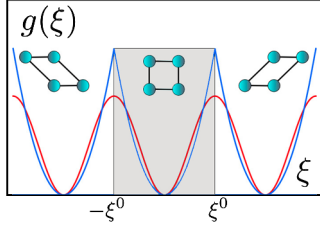


FIG. 1 (color online). Periodic dependence of energy on shear strain: continuous and piecewise quadratic potentials. One elastic domain is shadowed.

where now u is a lattice field, $[u]$ is a discrete increment, and the function ϕ is periodic with infinite symmetry group [22]. Assuming that the order parameter is scalar, one can minimize out remaining linear strain variables: the simplest example of the resulting dressed description is the one-dimensional FK model. Our minimal 2D setting can be viewed as an array of coupled FK chains with the energy [19,20] $\Phi(u) = \sum_{i,j} \phi(\theta, \xi)$, where $\theta(i, k) = u(i+1, k) - u(i, k)$ is an axial strain and $\xi(i, k) = u(i, k+1) - u(i, k)$ is a shear strain; the displacement field $u(i, k)$ is defined on a $N \times N$ square lattice ($a = 1$). The potential ϕ is assumed to be quadratic in θ and periodic in ξ (see Fig. 1); to avoid synchronization we also added quenched disorder $\phi(\theta, \xi) = g(\xi) + \frac{K}{2}(\theta)^2 - h_1\xi - h_2\theta$, where $h_{1,2}(i, j)$ are independent Gaussian random variables. Observe that the variables θ and ξ are not independent and the long-range interactions can be revealed through minimizing out the nonorder parameter variable θ [23].

The dynamic equations are taken in the form of the overdamped gradient flow $\nu \dot{u} = -\partial\Phi(u)/\partial u$, where ν is the ratio of the internal time scale and the time scale of the driving [17]. The driving in shear is performed through the displacement controlled boundary condition $\sum_{k=0}^{N-1} \xi(i, k) = t$, where t is the slow time playing the role of loading parameter; in the longitudinal direction we assume the periodic boundary condition $\sum_{i=0}^{N-1} \theta(i, k) = 0$. In our numerical experiments we took $K = 2$, $N = 512$, and $g(\xi) = (2\pi)^{-2}[1 - \cos(2\pi\xi)]$. The initial state was dislocation-free and the dispersion of disorder varied in the range 0.01–0.2. For computations we used an implicit-explicit fast-Fourier-transform method [24].

The results of direct numerical simulations (automaton reduction is discussed later) are presented in Fig. 2(a), where we show the macroscopic strain-stress curves covering the first two cycles of loading and unloading in the hard device. Notice that hysteresis loops converge, indicating that the system exhibits plastic shakedown. Reaching steady state is marked by the stabilization of dislocation density, which also shows a characteristic nucleation related overshoot [see Fig. 2(b)]. Steady state yielding is characterized by the formation of stable dislocation structures (cells) with plastic activity limited to intermittent dislocational exchanges between the clusters; the latter remain mostly stable from one cycle to another but have

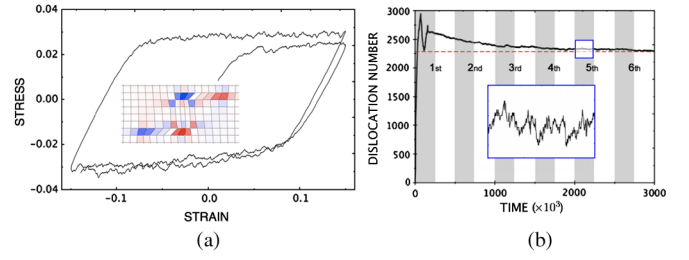


FIG. 2 (color online). (a) Macroscopic strain-stress curve showing plastic hysteresis and shakedown. The inset illustrates a fragment of the deformed lattice with two dislocation dipoles nucleated around an imperfection: red and blue colors correspond to dislocations of different sign. (b) Evolution of dislocation density with cycling. The inset shows fluctuations.

a finite lifetime as in observations [25]. To separate individual avalanches we introduce an irrelevant threshold and define the avalanche energy by integrating viscous dissipation over its duration: $E = N^{-2} \sum_{i,j} \int \dot{u}^2 dt$. We observe that the probability distribution $P(E)$ stabilizes after several cycles (see Fig. 3), exhibiting a robust power law behavior with exponent $\epsilon \approx 1.6 \pm 0.05$ obtained by the maximum likelihood method [26]. This value is in perfect agreement with experiments in ice crystals and fits the generally accepted range of 1.4–1.6 [1,6]; most remarkably, it is also consistent with the value obtained for 2D colloidal crystals [27]. The approximate proportionality between the plastic slip size and the dissipated energy ensures that acoustic emission measurements would exhibit the same exponent ϵ .

The spatial counterpart of the observed time correlations is the fractal structure of dislocational patterns. The dislocation rich regions (clusters) can be identified by the localized peaks of the energy density landscape [see inset in Fig. 4(a)], and the corresponding probability density shows a power law structure with exponent 1.45 ± 0.1 [Fig. 4(a)]. Another way to quantify the fractal clustering is to compute the correlation function of the dislocation distribution $C(r) \sim r^D$ [28]. We observe that during the first loading cycle $D \sim 2.0$, which is expected

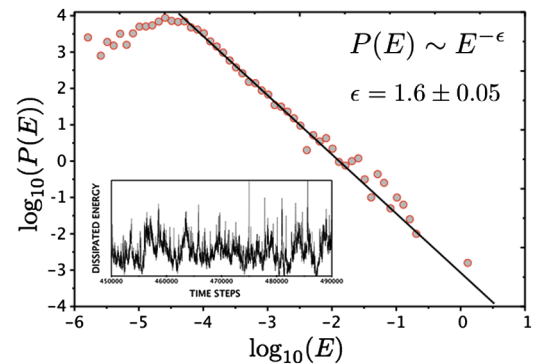


FIG. 3 (color online). Probability distribution of dissipated energy in a steady state; the inset shows the structure of fluctuations during a typical cycle.

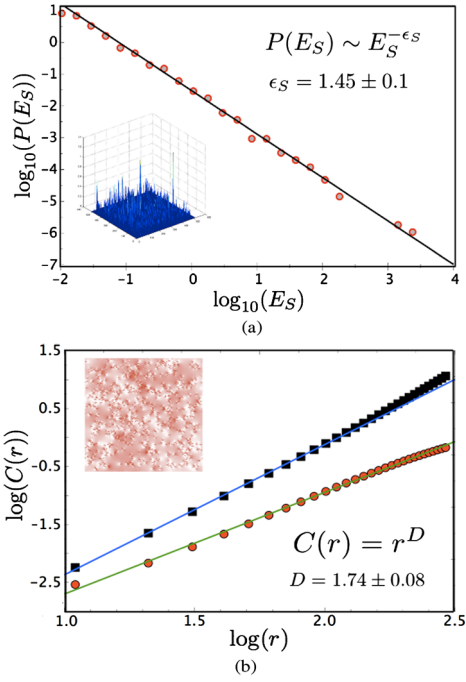


FIG. 4 (color online). (a) Probability distribution of dislocation rich regions in the shakedown state; the inset shows spatial distribution of the energy density $\phi(\theta, \xi)$. (b) Correlation function $C(r)$ after the first cycle (squares) and after the fifth cycle (circles); the inset shows a characteristic stress field during steady yielding.

given the random nature of the quenched disorder. With cycling the long-range correlations develop [see Fig. 4(b)], and in the shakedown regime we record $D \sim 1.74$ independently of initial disorder. Note that dislocation patterns with $D \approx 1.64$ – 1.79 have been observed experimentally in crystals with multiple slip systems; in simulations with a single slip system, fractal patterning has been previously linked to the possibility of dislocation multiplication [29], which is operative in our model.

Despite the conceptual transparency of the above model, the mechanism of reaching the critical regime remains obscure. The model, however, can be simplified further if we notice that in the quasistatic limit $\nu \rightarrow 0$ the relaxation is instantaneous and the system remains almost always in equilibrium $\partial\Phi/\partial u = 0$. In order to solve the equilibrium equations analytically, we can replace the smooth periodic potential by a piecewise quadratic potential (see Fig. 1) defined in each period $[(d-1)\xi^0, (d+1)\xi^0]$ as $g(\xi) = \frac{1}{2}(\xi - d)^2$, where d is the new integer-valued spin variable describing a quantized slip; since at given lattice field $d(i, j)$ the equilibrium equations are linear, the strain field can be found analytically (cf. [30]). The Fourier image $\hat{\xi}(\mathbf{q})$ of the shear strain $\xi(i, j)$ reads $\hat{\xi}(\mathbf{q}) = (s_y^+(\mathbf{q}) s_y^-(\mathbf{q}) \hat{d}(\mathbf{q}) + \hat{H}(\mathbf{q})) / \hat{\lambda}(\mathbf{q})$, where $\mathbf{q} = (q_x, q_y) = (2\pi k/N, 2\pi l/N)$ is the wave number. Here we defined $\hat{H}(\mathbf{q}) = s_x^-(\mathbf{q}) s_x^+(\mathbf{q}) \hat{h}_1(\mathbf{q}) + s_y^-(\mathbf{q}) s_y^+(\mathbf{q}) \hat{h}_2(\mathbf{q})$ and $\hat{\lambda}(\mathbf{q}) = 2K[\cos(q_x) - 1] + s_y^-(\mathbf{q}) s_y^+(\mathbf{q})$, where $s_a^\pm(\mathbf{q}) = \pm[1 - \cos(q_a) \pm i \sin(q_a)]$ with $a = x, y$. Notice also that we

control the average shear strain $\hat{\xi}_0(\mathbf{q}) = t\delta(\mathbf{q})$ and that the quenched disorder becomes the source of the residual strain $\hat{\xi}_h(\mathbf{q}) = \hat{H}(\mathbf{q})/\hat{\lambda}(\mathbf{q})$.

It is now straightforward to reformulate the model as an integer-valued automaton. Observe that the variable $\Delta\xi = \xi - (\xi_0 + \xi_h)$ representing shear strain fluctuations must be confined between the thresholds $-\xi^0 - \xi(h, t) < \Delta\xi(i, j) < \xi^0 - \xi(h, t)$, where $\xi(h, t) = [\hat{\xi}_h]_{\mathbf{q}}^{-1} + t$ and $[\cdot]_{\mathbf{q}}^{-1}$ denotes the inverse Fourier transform. When $\Delta\xi$ reaches the threshold, the integer parameter d is updated $d \rightarrow d + M(\Delta\xi)$, where

$$M(\Delta\xi) = \begin{cases} +1, & \text{if } \Delta\xi > \xi^t - \xi(h, t) \\ -1, & \text{if } \Delta\xi < -\xi^t - \xi(h, t) \\ 0, & \text{otherwise.} \end{cases}$$

After each increment of loading t we recheck the stability until all the units are stabilized; the dissipated energy during an avalanche is the difference of the total energies for two subsequent stable states.

The use of cellular automaton representation greatly reduces the complexity of numerical computations while the behavior of the system remains the same, including the shape of the stress strain hysteresis, the evolution of the dislocation density, and the structure of spatial and temporal correlations. To illustrate the statistics we show in Fig. 5 the finite-size scaling collapse of energy dissipation at the critical state; here we assumed that $P(E) = E^{-\epsilon} \varphi(E/E_c)$ with universal cutoff function φ and the cutoff energy which diverges in the thermodynamic limit as $E_c \sim N^\delta$. Our computations show that again $\epsilon \approx 1.6 \pm 0.05$ and that $\delta \approx 1.2 \pm 0.1$, which is close to the value $\delta \approx 1$ obtained for plastic strain increments in [6,31]. These exponents are insensitive to the degree of disorder in the studied range; for larger disorder we observed a cutoff which is no longer size dependent. Based on our computations we conclude that both models, the one with continuous dynamics and smooth potential and the one with discrete dynamics and piecewise quadratic potential, belong to the same universality class. This behavior is markedly different from the

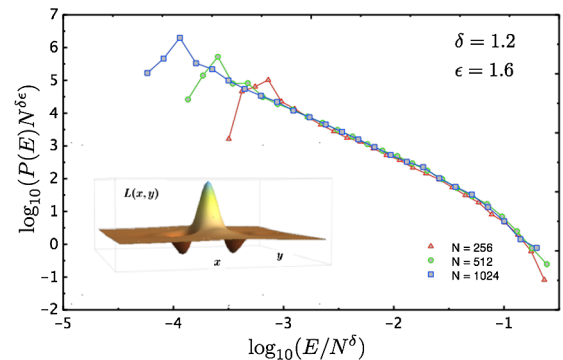


FIG. 5 (color online). Scaling collapse of the dissipated energy in automaton model for different system sizes N . The inset displays the kernel $L(x, y)$.

prediction of the mean field theory where smooth and cusped potentials lead to different universality classes [32].

An important question is whether the toppling rules in our automaton are Abelian, meaning that the outcome of the instability in multiple sites does not depend on the toppling order. The update of the “slope” field $\Delta\xi$ can be represented in Fourier space as $\hat{\Delta\xi} \rightarrow \hat{\Delta\xi} - \hat{L}(\mathbf{q})\hat{M}(\Delta\xi)$, where

$$\hat{L}(\mathbf{q}) = \frac{\sin(q_y/2)^2}{\sin(q_y/2)^2 + K \sin(q_x/2)^2}$$

is the analog of the toppling matrix in the sandpile models. The corresponding kernel $L(x, y)$ in the real space is highly anisotropic, long range, and conservative (see inset in Fig. 5). We compared numerically all conventional updating strategies and found that the microscopic configuration shows some small dependence on the choice of the strategy while the macroscopic observables, including the shake-down hysteresis loop and the statistics of avalanches (critical exponents), remain unaffected. One can conclude that our automaton has a weak (statistical) form of Abelian symmetry which may still be helpful for the mathematical analysis [15]. Another important property of our automaton model is that it necessarily lowers the energy during each avalanche. The dissipative structure is obvious in the continuum model and is inherited by the automaton model.

In conclusion, to elucidate the origin of self-organized criticality in plasticity we reduced a realistic continuous dynamics to an integer automaton by replacing the fast dissipative stages with jump discontinuities controlled by random thresholds. The fact that despite the long-range character of elastic interaction the computed exponents are different from the predictions of the mean field theory may mean that at least for some crystal classes plasticity is effectively a 2D phenomenon lying below the upper critical dimension.

The authors would like to thank A. Constantinescu, S. Conti, A. Finel, S. Papanikolaou, F.J. Perez-Reche, S. Roux, E. Vives, J. Weiss, S. Zapperi, and an anonymous reviewer for helpful discussions. This work was supported by the French ANR-2008 grant EVOCRIT.

-
- [1] T. Richeton *et al.*, *Nature Mater.* **4**, 465 (2005); D.M. Dimiduk *et al.*, *Science* **312**, 1188 (2006); M. Zaiser *et al.*, *Philos. Mag.* **88**, 3861 (2008); S. Brinckmann, J. Y. Kim, and J.R. Greet, *Phys. Rev. Lett.* **100**, 155502 (2008); D.M. Dimiduk *et al.*, *Philos. Mag.* **90**, 3621 (2010).
- [2] Y.S. Chen *et al.*, *Phys. Rev. Lett.* **105**, 105501 (2010).
- [3] H. Jensen, *Self-Organized Criticality* (Cambridge University Press, Cambridge, England, 1998); D.L. Turcotte, *Rep. Prog. Phys.* **62**, 1377 (1999); R. Dickman *et al.*, *Braz. J. Phys.* **30**, 27 (2000); J.P. Sethna, *Nature Phys.* **3**, 518 (2007); M. Henkel *et al.*, *Non-Equilibrium Phase Transitions* (Springer, New York, 2008).

- [4] M. Zaiser, *Adv. Phys.* **55**, 185 (2006); J. Weiss, *Surv. Geophys.* **24**, 185 (2003).
- [5] M.C. Miguel *et al.*, *Nature (London)* **410**, 667 (2001); M.C. Miguel *et al.*, *Phys. Rev. Lett.* **89**, 165501 (2002).
- [6] F.F. Csikor *et al.*, *Science* **318**, 251 (2007).
- [7] B. Devincre *et al.*, *Science* **320**, 1745 (2008).
- [8] P. Moretti *et al.*, *Phys. Rev. B* **69**, 214103 (2004).
- [9] M. Koslowski, R. LeSar, and R. Thomson, *Phys. Rev. Lett.* **93**, 125502 (2004).
- [10] K. Chen, P. Bak, and S.P. Obukhov, *Phys. Rev. A* **43**, 625 (1991); D.S. Fisher *et al.*, *Phys. Rev. Lett.* **78**, 4885 (1997); J.C. Baret, D. Vandembroucq, and S. Roux, *Phys. Rev. Lett.* **89**, 195506 (2002); C. Fressengeas *et al.*, *Phys. Rev. B* **79**, 014108 (2009); K.A. Dahmen, Y. Ben-Zion, and J.T. Uhl, *Phys. Rev. Lett.* **102**, 175501 (2009).
- [11] S. Papanikolaou *et al.*, *Nature Phys.* **7**, 316 (2011).
- [12] M. Zaiser and P. Moretti, *J. Stat. Mech.* (2005) P08004.
- [13] D. Dhar and S.N. Majumdar, *J. Phys. A* **23**, 4333 (1990); B. Alessandro *et al.*, *J. Appl. Phys.* **68**, 2901 (1990); S. Zapperi *et al.*, *Phys. Rev. B* **58**, 6353 (1998).
- [14] P. Le Doussal and K.J. Wiese, *Phys. Rev. E* **79**, 051106 (2009).
- [15] D. Dhar, *Physica (Amsterdam)* **263A**, 4 (1999).
- [16] O. Narayan and A.A. Middleton, *Phys. Rev. B* **49**, 244 (1994).
- [17] G. Puglisi and L. Truskinovsky, *J. Mech. Phys. Solids* **53**, 655 (2005); F.J. Pérez-Reche, L. Truskinovsky, and G. Zanzotto, *Phys. Rev. Lett.* **99**, 075501 (2007); A. Mielke and L. Truskinovsky, WIAS Report No. 1541, 2010.
- [18] P.D. Ispánovity *et al.*, *Phys. Rev. Lett.* **105**, 085503 (2010).
- [19] H. Suzuki, *Dislocation Dynamics* (McGraw-Hill, New York, 1968), p. 679; A.I. Landau *et al.*, *Phys. Status Solidi B* **179**, 373 (1993).
- [20] A. Carpio and L.L. Bonilla, *Phys. Rev. B* **71**, 134105 (2005); I. Plans *et al.*, *Europhys. Lett.* **81**, 36001 (2008); O. Kresse and L. Truskinovsky, *Izv. Russ. Acad. Sci. Phys. Solid Earth* **43**, 63 (2007).
- [21] O. Kresse and L. Truskinovsky, *J. Mech. Phys. Solids* **52**, 2521 (2004); L. Truskinovsky and A. Vainchtein, *Continuum Mech. Thermodyn.* **22**, 485 (2010).
- [22] S. Conti and G. Zanzotto, *Arch. Ration. Mech. Anal.* **173**, 69 (2004); F.J. Pérez-Reche *et al.*, *Continuum Mech. Thermodyn.* **21**, 17 (2009).
- [23] S. Kartha *et al.*, *Phys. Rev. B* **52**, 803 (1995); K.O. Rasmussen *et al.*, *Phys. Rev. Lett.* **87**, 055704 (2001).
- [24] R.J. LeVeque, *Finite Difference Methods for Ordinary and Partial Differential Equations* (SIAM, Philadelphia, PA, 2007).
- [25] B. Jakobsen *et al.*, *Science* **312**, 889 (2006).
- [26] A. Clauset *et al.*, *SIAM Rev.* **51**, 661 (2009).
- [27] A. Pertsinidis and X.S. Ling, *New J. Phys.* **7**, 33 (2005).
- [28] H. Hentschel and I. Proccacia, *Physica (Amsterdam)* **8D**, 435 (1983).
- [29] P. Hahner, K. Bay, and M. Zaiser, *Phys. Rev. Lett.* **81**, 2470 (1998); B. Bakó and I. Groma, *Phys. Rev. B* **60**, 122 (1999); I. Groma and B. Bakó, *Phys. Rev. Lett.* **84**, 1487 (2000); J. Weiss and A. Marsan, *Science* **299**, 89 (2003).
- [30] A. Koslowski *et al.*, *J. Mech. Phys. Solids* **50**, 2597 (2002).
- [31] M. Zaiser and N. Nikitas, *J. Stat. Mech.* (2007) P04013.
- [32] D.S. Fisher, *Phys. Rev. B* **31**, 1396 (1985); O. Narayan and D.S. Fisher, *Phys. Rev. B* **48**, 7030 (1993).